The Effect of Roughness on the Convective Stability of the Rotating Disk Boundary Layer

P.Y.A.G.S. Yapa[1*], S.J. Garrett [2], P.T. Griffiths[3] and P.J. Thomas[4]

[1]Department of Mathematics and Philosophy of Engineering, The Open University of Sri Lanka, Nawala, Nugegoda, Sri Lanka
[2]School of Engineering, University of Leicester, Leicester, LE1 7RH, UK
[3]School of Computing, Electronics and Mathematics, Faculty of Engineering, Environment and Computing, Coventry University, Coventry, CV1 5FB, UK
[4]Fluid Dynamics Research Centre, School of Engineering, University of Warwick, Coventry, CV4 7AL, UK.

*Corresponding Author: email: yayap@ou.ac.lk, Tele: +94112881441

Abstract *– A numerical analysis of the impact of surface roughness, both anisotropic and isotropic, on the convective stability of the boundary-layer flow over a rotating disk is presented. Surface roughness is modelled by means of specifying partial-slip, instead of no slip, on the disk surface. Linear stability analysis is performed to identify how roughness affects the stability characteristics of the inviscid Type I (or cross-flow) instability and the viscous Type II instability that arise in the rotating-disk boundary layer and examine how the neutral stability curves vary with different levels of roughness for this roughness-modelling approach. Stationary modes are studied and both anisotropic (concentric grooves and radial grooves) and isotropic roughness are shown to have a stabilizing effect on the Type I instability. It is demonstrated that radial grooves on the disk surface have a strongly destabilizing effect for Type II, whereas concentric grooves and isotropic roughness have a stabilizing effect for Type II instability. It appeared sensible to expect that the spatial location of the point of inflection on the radial velocity profile could be closely related to the laminar-turbulent transition behavior. Therefore, an analysis of the variation of the location of the inflection point is presented. In order to reconfirm the results of the linear stability analysis, drag or moment coefficients were calculated as a surface integral of shear stress. The data displayed shifts downward with increasing isotropic roughness levels and radial grooves. That is, the torque decreases, and this behavior implies drag reduction. However, data lines are shifted upwards for the case of concentric grooves. That, conversely, implies a drag increase, with increasing levels of azimuthal roughness.*

Keywords*: Aerodynamics; Wall-boundary flows, rotating disk flow*

Nomenclature

C_M - Moment coefficient
u^* - Radial velocity
v^* - Azimuthal velocity
w^* - Axial velocity
M – Resisting torque
Re – Reynolds number
n – Spiral vortices
$*$ - Dimensional quantity

Greek Letters
Ω^*- Angular velocity
ν^* - Kinematic viscosity
λ – Radial roughness
η - Azimuthal roughness
α – Radial wave number
β – Circumferential wave number
γ – Frequency
τ – Shear stress
μ - Coefficient of viscosity of fluid

1 INTRODUCTION

Viscous shear forces acting on the surface of a rigid body cause skin-friction drag when the body moves through a fluid. In most technological applications, this drag increases as the flow transitions from laminar to turbulent and finding a way to reduce drag has been a research priority for many years (Alveroglu et al. 2016, Sirovich and Karlson 1997, Choi 2006). The *right sort of roughness* (Carpenter 1997) can reduce drag.

As part of recent theoretical studies (Cooper et al. 2015, Garrett et al. 2016, Özkan et al. 2017) the Warwick group investigated roughness effects on boundary-layers with a crossflow component as established over a rotating disk (cf. Fig. 1). The basic flow geometry is schematically illustrated in Fig.1, where the flow established by a disk of radius, R that rotates with velocity, Ω, in an ambient environment of an incompressible fluid of viscosity, ν.

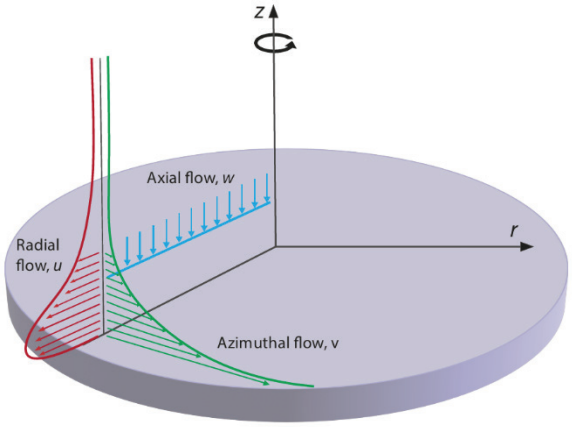

Fig. 1. Boundary-layer velocity components of rotating disk flow.

The fluid is at rest infinitely far above the disk. Due to the no-slip condition on the disk surface, a thin boundary layer is established above the surface of the disk. The azimuthal motion around the axis of rotation is, hereinafter referred to as v. Centripetal forces result in a flow component directed radially outwards, u. This flow component is commonly referred to as the cross-flow component. Due to the requirement for mass conservation, the radial component of the flow velocity necessitates, in turn, a down-flow component towards the disk, w.

Thus, the boundary-layer flow is fully three dimensional. Its particular characteristic, that distinguishes it from many other types of boundary layers is the cross-flow component. Similar boundary-layer flows with a cross-flow exist over components of rotating machinery or over highly swept wings of aeroplanes (Lingwood and Henrik 2015, Saric et al. 2003, Wimmer 1988).

The pioneering study which addresses the rotating disk boundary-layer was performed by Theodore von Kármán (1921) who formulated the problem. He established that there exists an exact similarity solution to the Navier-Stokes equation and calculated the resulting velocity profiles for the azimuthal, radial and axial boundary-layer velocity components.

A linear stability analysis can then be performed to investigate the effect of roughness on the convective instability characteristics of the inviscid Type I (cross-flow) instability and the viscous Type II instability. Type I mode arises as a consequence of the inflection point on the cross-flow velocity profile and Type II mode arises from streamline curvature and Coriolis effects (Cooper et al. 2015, Lingwood 1995, Malik 1986).

Lord Rayleigh (1879) established that a necessary condition, for an equilibrium flow to become unstable, is that the equilibrium velocity distribution must contain an inflection point. Such an inflection point, on the mean radial flow profile, over a rotating disk is considered to be the

direct cause of the so-called cross-flow instability. Any changes in the location of the inflection point could affect the behaviour of the instability in turn.

In order to extract possible underlying physical mechanisms behind the effects of roughness, drag or moment coefficients, C_M were calculated.

2 FORMULATION OF THE PROBLEM

Von Kármán considered the infinite disk rotating with constant angular velocity Ω^* in a fluid of kinematic viscosity ν^*. Let (u^*, v^*, w^*) be the velocity components in the cylindrical coordinates (r^*, θ, z^*) respectively. Equation (1) illustrates the use of the similarity transformation.

$$[u^*, v^*, w^*] = \left[r^*\Omega^* u(z), r^*\Omega^* v(z), (\nu^*\Omega^*)^{1/2} w(z)\right] \tag{1}$$

where $z = z^*\sqrt{\Omega^*/\nu^*}$, the asterisks denote the dimensional form of the quantities.

The Navier-Stokes equations reduce to the non-linear ordinary differential equations (Schlichting 1968), as shown by Equations (2)-(4).

$$u^2 - (v+1)^2 + u'\, w - u''\, = 0 \tag{2}$$

$$2u\,(v+1) + v'\, w - v''\, = 0 \tag{3}$$

$$2u + w' = 0 \tag{4}$$

Navier (1827) proposed the partial-slip condition for rough surfaces, in the radial and azimuthal directions. This approach was adopted by Miklavčič and Wang (2004) who assume that roughness over a rotating disk can be modelled by a modification of the no-slip conditions at the disk surface. In Equations (5) and (6), the modified wall boundary conditions are represented.

$$u(0) = \lambda\, u'\,(0) \tag{5}$$

$$v(0) = \eta\, v'\,(0) \tag{6}$$

where primes denote differentiation with respect to z, and the two parameters λ and η give empirical measures of the roughness in the radial and azimuthal directions, respectively. The case $\lambda = \eta = 0$ represents the no-slip boundary conditions for a smooth disk. Isotropic roughness is represented by cases with $\lambda = \eta > 0$. Values of $\lambda > 0, \eta = 0$ describe anisotropic roughness that can be interpreted as concentric grooves, whereas $\eta > 0, \lambda = 0$ represents the anisotropic roughness that can be interpreted as radial grooves.

3 THE MEAN FLOW SOLUTIONS

The purpose of this section is to present the solutions of the steady mean flow equations with the aim of investigating the effects of both isotropic and anisotropic surface roughness on the mean flow profiles of the von Kármán boundary layer.

The isotropic surface roughness corresponds to equally distributed roughness in the radial and azimuthal directions on the disk surface (Fig. 2(a)). The radially anisotropic surface roughness represents a pattern of concentric circles – concentric grooves – on the disk (Fig. 2(b)). The azimuthally anisotropic surface roughness corresponds to radial grooves on the disk surface (Fig. 2(c)).

(a) (b) (c)

Fig. 2. Distribution of roughness over a disk. (a) Isotropic roughness, (b) concentric grooves and (c) radial grooves.

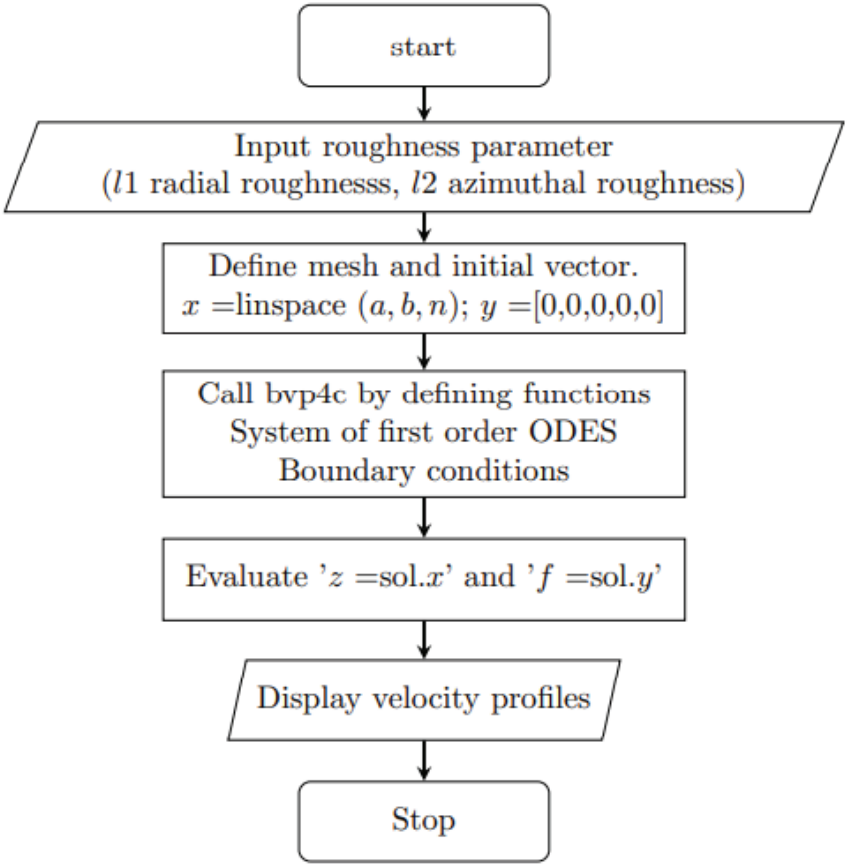

Fig. 3. A Flow chart of bvp4c method.

The MATLAB function bvp4c, which is described in (Yapa 2023), is used to solve the governing equations of the steady mean flow profiles. The bvp4c sequence is shown in Fig. 3. Computational results for the mean flow profiles for various roughness levels are discussed. The radial mean flow component U is presented in Figs. 4(a)-(c), the azimuthal mean flow profile V is shown in Figs. 5(a)-(c) and the axial flow component W is displayed in Figs. 6(a)-(c). The initial values of $U^{'}(0)$ and $V^{'}(0)$ are important for the computation of the flow profiles. They are shown in Table 1 for various roughness levels. Our initial values for the von Kármán flow are identical to those presented by Miklavčič and Wang (2004). $V^{'}(0)$ for various roughness levels is a crucial factor used for the calculation of C_M (Refer Equation A6).

The important properties of the mean flow profiles, which are potentially affected by increased surface roughness are the boundary layer thickness, the size of the radial wall jet and the amount of fluid entrained into the boundary layer. The size of the radial wall jet depends on the maximum value of radial component U in the flow field. The amount of fluid entrained into the boundary layer is prescribed by the value of the axial flow component W.

Fig. 4(a) displays results for the isotropic case. The figure reveals that the maximum radial velocity reduces with increasing roughness. Simultaneously the height above the disk where the maximum velocity occurs moves closer to the disk surface. Fig. 4(b) shows results for the case of anisotropic roughness with concentric grooves. Inspection of the figure shows that increasing slip in the radial direction results in an increase of the maximum radial velocity. Fig. 4(c) shows results for the case of radial grooves. Here an increase of the slip in the azimuthal direction leads to a decrease of the maximum radial velocity.

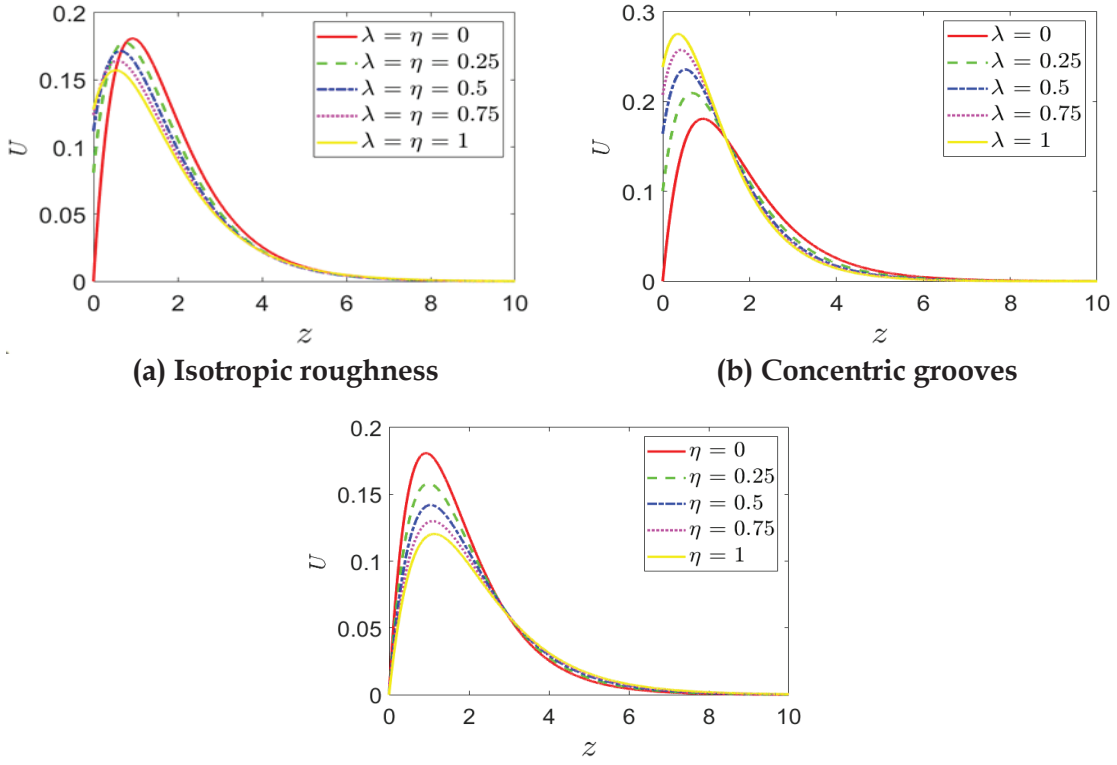

(a) Isotropic roughness **(b) Concentric grooves**

(c) Radial grooves

Fig. 4. Steady flow profiles, radial velocity profile U.

For the isotropic case, Fig. 5(a) shows that the azimuthal velocity value decreases with increasing roughness. For the case of anisotropic roughness with concentric grooves Fig. 5(b) illustrates that increasing slip in the radial direction does not result in notable changes of the azimuthal velocity. Fig. 5(c) finally shows that, for the case of radial grooves, increasing slip in the azimuthal direction leads to a decreasing azimuthal velocity.

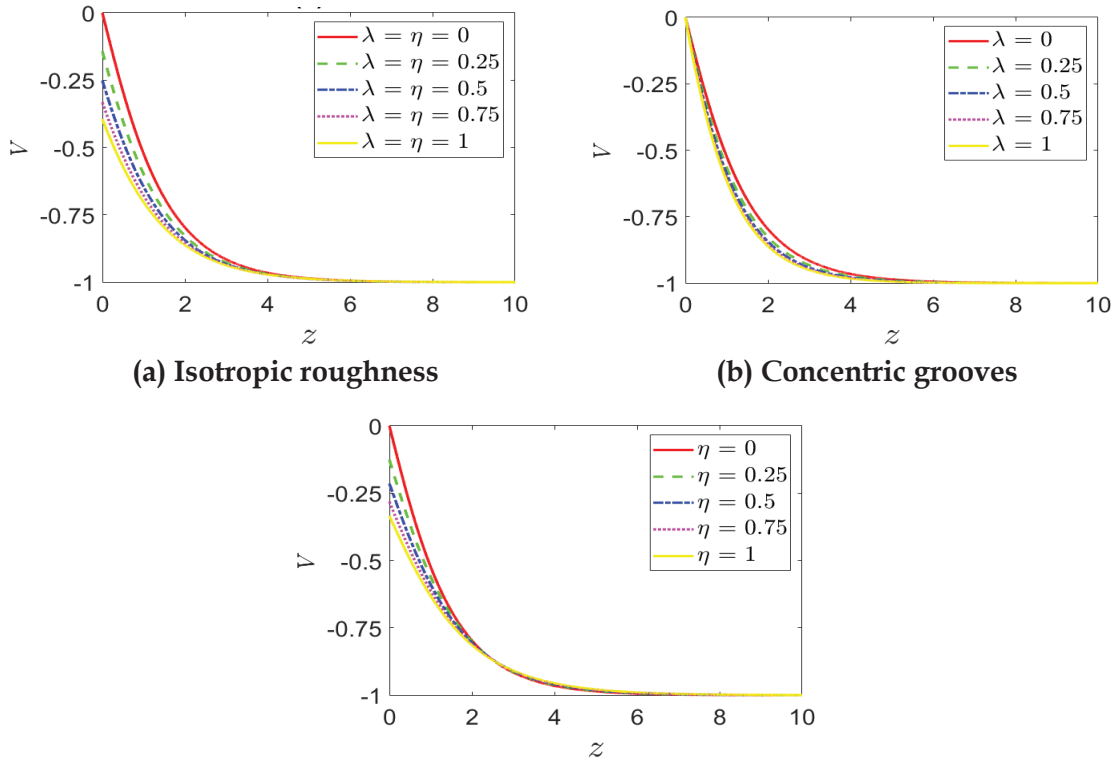

(a) Isotropic roughness **(b) Concentric grooves**

(c) Radial grooves

Fig. 5. Steady flow profiles, azimuthal velocity profile V.

The resisting torque M given in appendix (Equation A4) is related to the initial values of the derivatives of azimuthal velocity components. Calculated C_M using Equation (A6) for various roughness levels are presented in Table 1. Miklavčič and Wang (2004) reported that, in von Kármán flow, increasing λ raises the torque, while increasing η reduces it, consistent with the data in Table 1.

Table 1: The initial values of U' and V' at the disk surface for various levels of roughness and moment coefficient, C_M.

(a) Isotropic roughness

Parameter	**U′(0)**	**V′(0)**	**C_M**
$\lambda = \eta = 0$	0.51023262	-0.61592201	1.935
$\lambda = \eta = 0.25$	0.32420081	-0.57061064	1.792
$\lambda = \eta = 0.5$	0.22384821	-0.5028097	1.58
$\lambda = \eta = 0.75$	0.16519178	-0.44341133	1.393
$\lambda = \eta = 1$	0.12792364	-0.39492759	1.241

(a) Concentric grooves

Parameter	U′(0)	V′(0)	C_M
$\lambda = 0$	0.51023262	-0.61592201	1.935
$\lambda = 0.25$	0.40177245	-0.72505447	2.278
$\lambda = 0.5$	0.32839517	-0.79138708	2.486
$\lambda = 0.75$	0.27661288	-0.83513295	2.624
$\lambda = 1$	0.23848733	-0.86588962	2.72

(a) Radial grooves			
Parameter	$U'(0)$	$V'(0)$	C_M
$\boldsymbol{\eta = 0}$	0.51023262	-0.61592201	1.935
$\boldsymbol{\eta = 0.25}$	0.41701212	-0.50339185	1.581
$\boldsymbol{\eta = 0.5}$	0.35526233	-0.42885125	1.347
$\boldsymbol{\eta = 0.75}$	0.31081455	-0.37519657	1.179
$\boldsymbol{\eta = 1}$	0.27704735	-0.33443486	1.05

The profiles for the axial velocity in the case of isotropic roughness in Fig. 6(a) shows that overall, there is less fluid entrainment into the boundary layer compared to the smooth disk. For the case of anisotropic roughness with concentric grooves, as the slip in the radial direction increases the entrainment of fluid into the boundary layer is increased as seen in Fig. 6(b). For the case of radial grooves, as the slip in the azimuthal direction increases entrainment of fluid into the boundary layer is reduced as seen in Fig. 6(c).

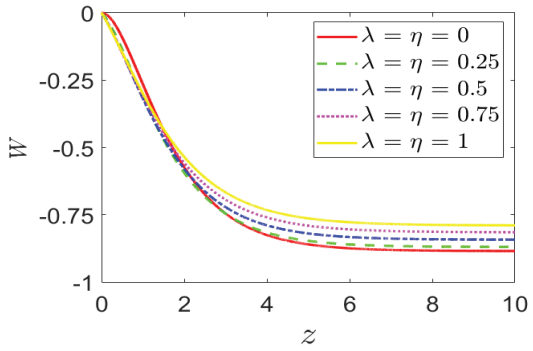

(a) Isotropic roughness

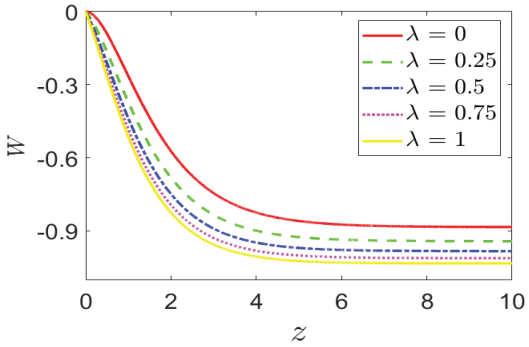

(b) Concentric grooves

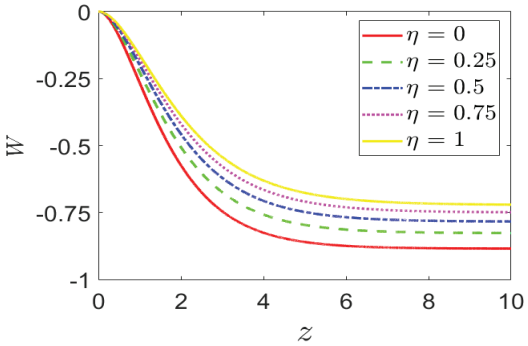

(c) Radial grooves

Fig. 6. Steady flow profiles, axial velocity profile *W*.

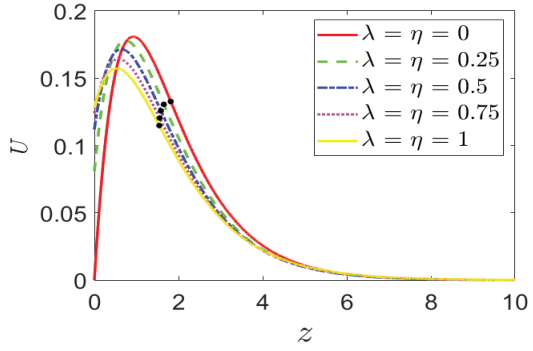

(a) Isotropic roughness

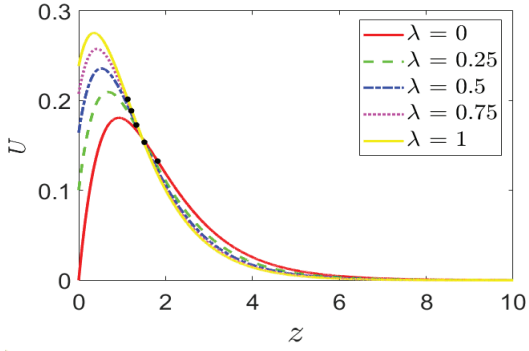

(b) Concentric grooves

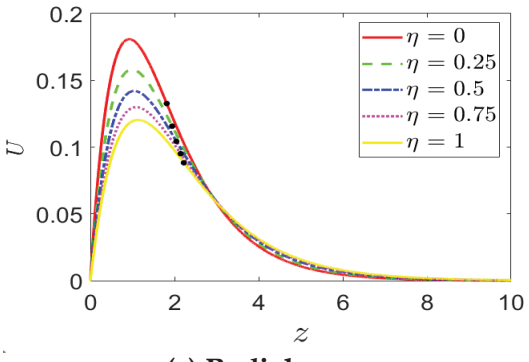

(c) Radial grooves

Fig. 7. Steady flow profiles, radial velocity profile U showing the points of inflection.

4 INFLECTION POINT VARIATION ANALYSIS

This section presents the spatial location of the inflection point on the radial velocity profile. In Figs. 7(a)–(c), the inflection point is marked by a black symbol on each curve. For the case of isotropic roughness Fig. 7(a) shows that increasing roughness leads to a decrease of the radial velocity at the inflection point. Fig. 7(b), for anisotropic roughness with concentric grooves reveals that increasing slip in the radial direction leads to a decrease of the radial velocity at the inflection point. Finally, for the case of radial grooves in Fig. 7(c), an increase of slip in the azimuthal direction results in a decrease of the radial velocity at the inflection point.

5 THE CONVECTIVE INTABILITY ANALYSIS

A convective instability is characterized by a disturbance that grows as it is convected away from its source. The flow at the disturbance location will in time return to a laminar state if not continuously disturbed. For the rotating disk boundary layer, the stationary vortices appearing around the disk in experiments are an example of a convective instability (Alveroglu 2016).

The resulting steady flow profiles are directly related to the von Kármán flow, and previous stability analysis for the rotating disk flow are applicable to this study (Lingwood 1995, Lingwood and Garrett 2011, Cooper and Carpenter 1997). Full details of the governing perturbation equations and the codes used can be found in those references.

The normal mode analysis is conducted with the perturbations of the form is illustrates in equation (7).

$$(\hat{u}, \hat{v}, \hat{w}, \hat{p}\ ) = \big(u(z), v(z), w(z), p(z)\big)e^{i(\alpha r + \beta Re\theta - \gamma t)} \tag{7}$$

The wave number in the radial direction, $\alpha = \alpha_r + i\alpha_i$, is complex, as required by the spatial convective analysis to be conducted; the frequency, γ, and the circumferential wave number, β, are real.

From the literature (Malik 1986, Gregory at el. 1955, Smith 1947, Gray 1952) it is known that there are two modes governing the convective instability properties of the disturbance modes over rough rotating disks. The Type I mode, appearing as the upper lobe in $\alpha - Re$ neutral curves, is known to arise from the inflectional nature of the steady-flow profiles, and the Type II mode, appearing as the lower lobe, is known to arise from streamline curvature and Coriolis effects. The characteristics of convective instability are examined in terms of neutral curves in 5.1.

5.1 Neutral Stability Curves (NSC)

In this section, the neutral curves for the boundary layer flows belonging to the von Kármán flow system are presented in the (Re, α) and (Re, n) planes for both the isotropic and anisotropic surface roughness. Figs. 8(a)-(c) show the neutral curves obtained for three cases, isotropic roughness, concentric grooves and radial grooves respectively in the $\alpha - Re$ plane. Figs. 9(a)-(c) show the neutral curves obtained for the same three cases in the $n - Re$ plane. These curves are consistent with those of Cooper et al. (2015). Note that in the Cooper et al paper, as well as in several other publications by different authors, there was an inconsistency as regards λ and η and their association with concentric and radial grooves. The correct interpretation is as follows. Since λ is the slip coefficient for the radial flow component it represents roughness in the radial direction. It can, therefore, be interpreted as concentric grooves. Similarly, η is the slip coefficient for the azimuthal flow component and represents roughness in the azimuthal direction. It can, therewith, be interpreted as radial grooves.

Fig. 8(a) and (b) illustrates that there exist strong stabilising effects on both the Type I and Type II modes in terms of the critical Reynolds number and the width of the instability region. The critical Reynolds number for the onset of the Type I and Type II modes increases with the roughness level. Furthermore, the width of instability region shrinks with an increase in the roughness level. Both are significant stabilising effects. Fig. 8(c) displays that strong stabilising effect on Type I mode in terms of the critical Reynolds number and the width of the instability region. In contrast Type II mode has destabilizing effect.

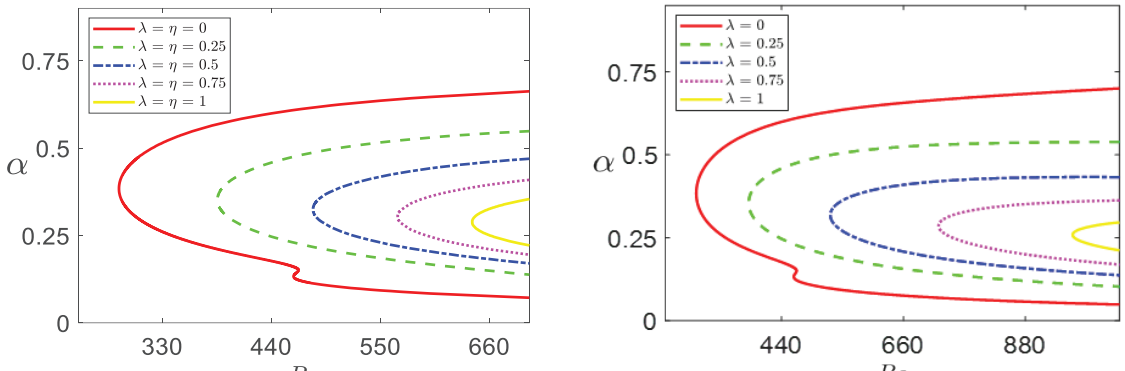

(a) Isotropic roughness **(b) Concentric grooves**

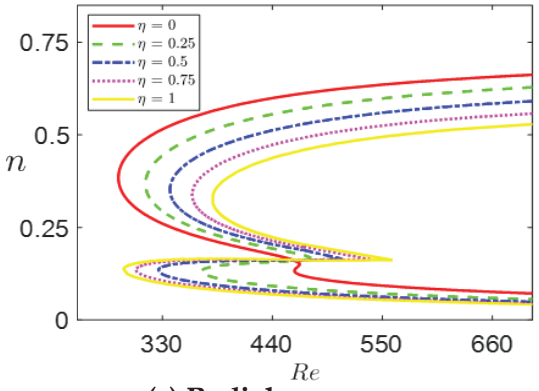

(c) Radial grooves

Fig.8. The radial wave number, α, as a function of Reynolds number, Re along the neutral curves.

The other parameter that is helpful to understand the effects of surface roughness is the number of the stationary vortices n. Figs. 9(a) and (b) display that the number of vortices increases along the upper branch of the neutral curves as roughness is increased in contrast to the strong stabilising effect on Type I mode. Fig. 9(c) shows that decreasing of the number of vortices n along both the upper and lower branches of the neutral curves with increased roughness; this is in parallel with the strong stabilising effect on the Type I mode.

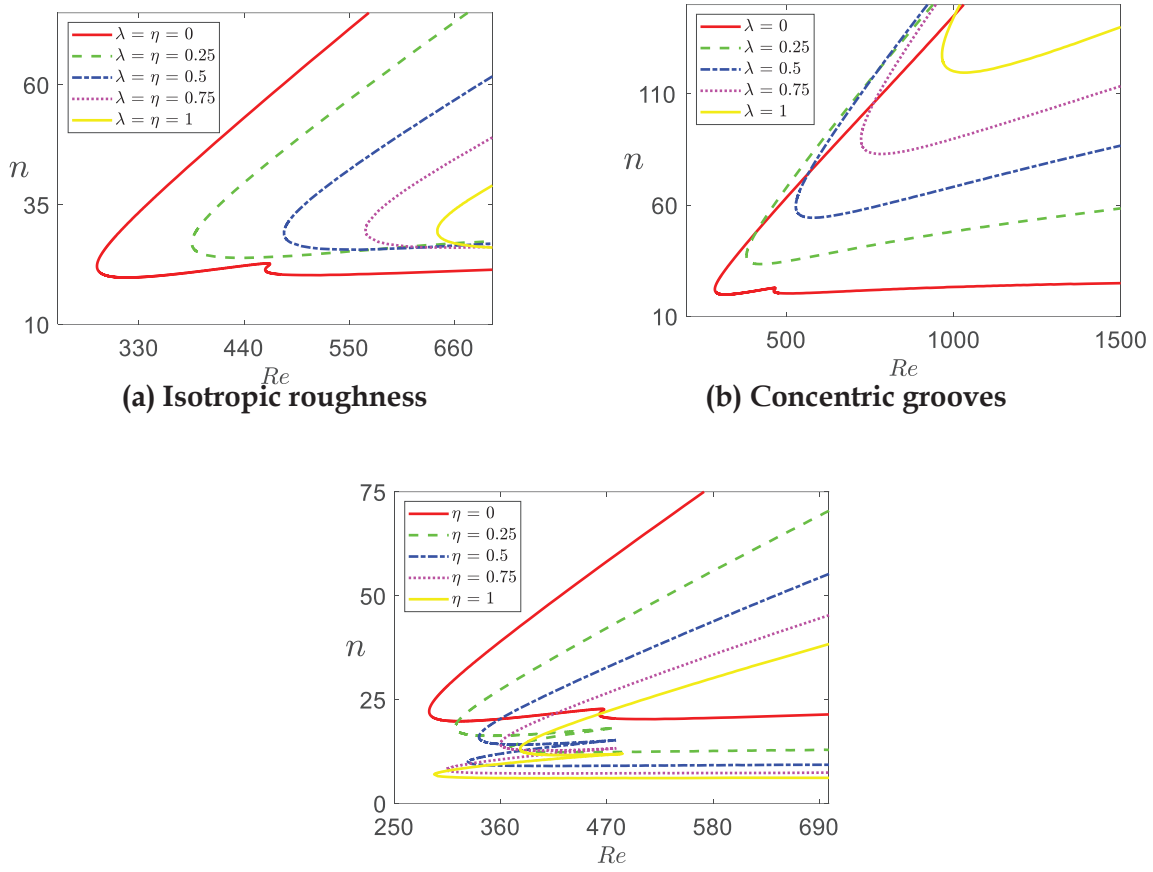

(a) Isotropic roughness **(b) Concentric grooves**

(c) Radial grooves

Fig. 9. The number of vortices, n, as a function of Reynolds number, Re along the neutral curves.

6 MOMENT COEFFICIENT ANALYSIS

This section addresses the results of the drag or moment coefficient (C_M), defined in Equation (A6). The moment coefficient, C_M, is plotted in Figs. 10(a)-(c) as a function of the Reynolds number Re. The data are displayed in double-logarithmic representation. The analytic expression for the resisting torque or moment on the rotating disks was derived here independently. To this end the stresses over the disk surfaces were integrated as shown in the appendix. The formulas obtained are in agreement with those given in Owen and Rogers (1989) and Theodorsen and Regier (1944).

Figs. 10(a) and (c) show that the lines displayed shift downwards, when the slip factor increases, and this behaviour can be interpreted as drag reduction. Whereas Fig. 10(b) shows drag increase, when the slip factor increases.

7. CONCLUSION

Computational data investigating the effects of both isotropic and anisotropic surface roughness on the convective stability of the von Kármán boundary-layer flow over a rotating

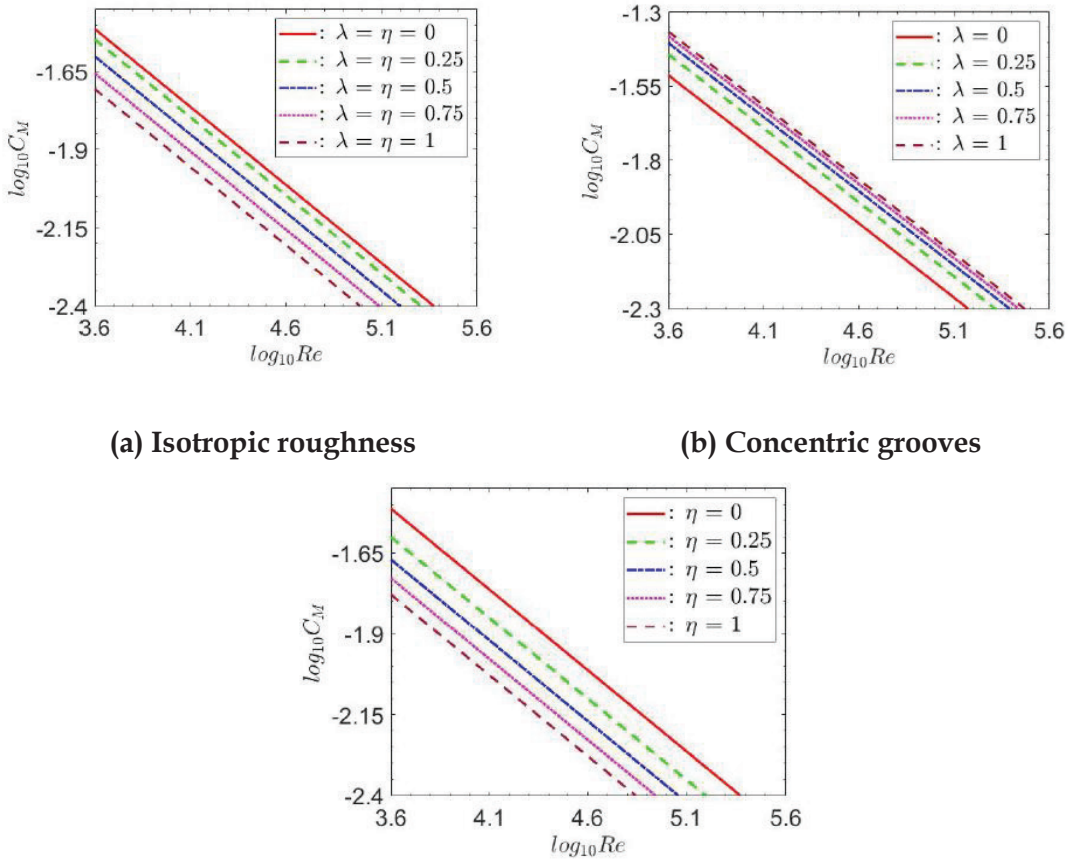

(a) Isotropic roughness **(b) Concentric grooves**

(c) Radial grooves

Fig. 10. The moment coefficient C_M for disks as a function of Reynolds number, Re.

disk was presented and discussed. The numerical analysis was based on the partial-slip approach for modelling the steady boundary-layer flow over a rough rotating disk. Results produce qualitatively consistent results with Cooper et al. (2015) for the three steady-flow velocity components of the rotating-disk boundary layer for increasing roughness levels.

The linear stability analysis based on the steady-flow profiles obtained reveals that both anisotropic and isotropic roughness result in a stabilization of the Type I instability mode, where the results of Cooper et al. (2015) are confirmed. It is shown that a disk with radial grooves has a strongly destabilizing effect, whereas a disk with concentric grooves and isotropic roughness have a stabilizing effect for the Type II instability.

The upward and downward trends seen in the location of the inflection point are not sufficient to make definitive conclusions regarding the boundary-layer stability.

The results presented have been supported by moment-coefficient calculations in order to explore the underlying physical mechanisms behind the stabilizing effects. The observed drag reduction for the cases of Isotropic roughness and radial grooves and drag increase for the case of concentric grooves, are not sufficient to evaluate the underlying physical mechanisms behind the stabilizing effects of surface roughness on the Type I and Type II instabilities.

Further analysis is required to find out the most effective type of distributed surface roughness in order to recommend as a passive-drag reduction mechanism for von Kármán flows in typical engineering applications.

ACKNOWLEDGEMENTS

This research is a part of the outcome of the PhD study of the first author. The first author acknowledges Prof. Peter J. Thomas for waving off the tuition fee for the PhD study. Additionally, this work was partially funded by the Open University of Sri Lanka and the University Grant Commission of Sri Lanka.

REFERENCES

Alveroglu, B., Segalini, A. and Garrett, S.J. (2016). The effect of surface roughness on the convective instability of the BEK family of boundary-layer flows. *European Journal of Mechanics - B/Fluids*, 56, pp.178–187.

Alveroglu, B. (2016). *The convective instability of the BEK system of rotating boundary-layer flows over rough disks*. Ph.D. thesis, University of Leicester, UK.

Carpenter, P.W. (1997). The right sort of roughness. Nature, 388, pp.713–714.

Choi, K.S. (2006). The rough with the smooth. *Nature*, 440, p.754.

Cooper, A.J., Harris, J.H., Garrett, S.J., Özkan, M. and Thomas, P.J. (2015). The effect of anisotropic and isotropic roughness on the convective stability of the rotating disk boundary layer. *Physics of Fluids*, 27, 014107.

Cooper, A.J. and Carpenter, P.W. (1997). The stability of rotating disc boundary layer flow over a compliant wall. Part 1. Types I and II instabilities. *Journal of Fluid Mechanics*, 350, pp.231–259.

Garrett, S.J., Cooper, A.J., Harris, J.H., Özkan, M., Segalini, A. and Thomas, P.J. (2016). On the stability of von Kármán rotating-disk boundary layers with radial anisotropic surface roughness. *Physics of Fluids*, 28, 014104.

Gray, W.E. (1952). The nature of the boundary layer flow at the nose of a swept wing. *Royal Aircraft Establishment Technical Memorandum*, 256.

Gregory, N., Stuart, J.T. and Walker, W.S. (1955). On the stability of three dimensional boundary layers with application to the flow due to a rotating disk. *Philosophical Transactions of the Royal Society of London. Series A: Mathematical, Physical and Engineering Sciences*, 248(943), pp.155–199.

Lingwood, R.J. and Henrik, A.P. (2015). Instabilities of the von Kármán boundary layer. Applied Mechanics Reviews, 67.

Lingwood, R.J. (1995). Absolute instability of the boundary layer on a rotating-disk. *Journal of Fluid Mechanics*, 299, pp.17–33.

Lingwood, R.J. and Garrett, S.J. (2011). The effects of surface mass flux on the instability of the BEK system of rotating boundary-layer flows. *European Journal of Mechanics - B/Fluids*, 30, pp.299–310.

Malik, M.R. (1986). The neutral curve for stationary disturbances in rotating-disk flow. *Journal of Fluid Mechanics*, 164, pp.275–287.

Miklavčič, M. and Wang, C.Y. (2004). The flow due to a rough rotating disk. *Zeitschrift für angewandte Mathematik und Physik (ZAMP)*, 55, pp.235–246.

Navier, C.L.M. (1827). Sur les lois du mouvement des fluides. *Comptes Rendus de l'Académie des Sciences*, 6, pp.389–440.

Özkan, M., Thomas, P.J., Cooper, A.J. and Garrett, S.J. (2017). Comparison of the effects of surface roughness and confinement on rotor-stator cavity flow. *Engineering Applications of Computational Fluid Mechanics*, 11, pp.142–157.

Owen, J.M. and Rogers, R.H. (1989). *Flow and heat transfer in rotating-disk systems. Volume 1: Rotor-Stator Systems*. Taunton, Somerset: Research Studies Press Ltd.

Rayleigh, L. (1879). On the stability, or instability, of certain fluid motions. *Proceedings of the London Mathematical Society*, 57.

Saric, W.S., Reed, H.L. and White, E.B. (2003). Stability and transition of three-dimensional boundary layers. *Annual Review of Fluid Mechanics*, 35, pp.413–440.

Schlichting, H. (1968). *Boundary-layer theory*. 6th ed. New York: McGraw-Hill.

Sirovich, L. and Karlson, S. (1997). Turbulent drag reduction by passive mechanisms. *Nature*, 388, pp.753–755.

Smith, N.H., (1947). Exploratory investigation of laminar-boundary-layer oscillations on a rotating disk. *NACA Report*.

Theodorsen, T. and Regier, A., (1944). Experiments on drag of revolving disks, cylinders, and streamline rods at high speeds. *NACA Report*, 793, p.367.

von Kármán, T., (1921). Über laminare und turbulente Reibung. *Zeitschrift für angewandte Mathematik und Mechanik*, 1, p.233.

Wimmer, M. (1988). Viscous flows and instabilities near rotating bodies. *Progress in Aerospace Sciences*, 25, pp.43–103.

Yapa, P.Y.A.G.S. (2023). Designing optimal roughness: A theory-led approach to roughness-based drag reduction. Ph.D. thesis, School of Engineering, University of Warwick, Coventry, UK. Available at: wrap.warwick.ac.uk/id/eprint/187476 [Accessed 29 June 2025].

APPENDIX

Here only an outline of the derivation procedure of moment coefficients will be provided, for details refer to (Yapa 2023). The local shear stress τ in the azimuthal direction is given by Newton's law of viscosity, where μ is the coefficient of viscosity.

$$\tau = \mu \left.\frac{\partial v^*}{\partial z^*}\right|_{z=0} \tag{A1}$$

By nondimensionalizing [fluid density (ρ)];

$$\tau = \rho\, r^*\, \Omega^*\, \sqrt{\nu^*\, \Omega^*}\; v'(z)\big|_{z=0} \tag{A2}$$

The total torque M is calculated as [Owen and Rogers 1989];

$$M = \int r^*\, \tau\, dA = -\rho\, \Omega^*\, \sqrt{\nu^*\, \Omega^*}\; v'(z)\big|_{z=0} \int_{\theta=0}^{\theta=2\pi} \int_{r^*=0}^{r^*=a} {r^*}^3 dr^*\, d\theta \tag{A3}$$

$$M = -\frac{1}{2}\pi\, \rho\, \Omega^{\frac{3}{2}}\, \nu^{\frac{1}{2}}\; a^4\, v'(z)\big|_{z=0} \tag{A4}$$

and the moment coefficient C_M is [Theodorsen and Regier 1994];

$$C_M = \frac{M}{\frac{1}{2}\,\rho\Omega^2\, a^5} \; and \; Re = \frac{\Omega\, a^2}{\nu} \tag{A5}$$

$$C_M = -\pi \left(v'(z)\big|_{z=0}\right) Re^{-\frac{1}{2}} \tag{A6}$$

In the above, Re denotes the Reynolds number based on the finite radius $r^* = a$.